AIP Applied Physics Letters

Controlling the plasmonic surface waves of metallic nanowires by transformation optics

Yichao Liu, Jun Yuan, Ge Yin, Sailing He, and Yungui Ma

Citation: Applied Physics Letters **107**, 011902 (2015); doi: 10.1063/1.4926332
View online: http://dx.doi.org/10.1063/1.4926332
View Table of Contents: http://scitation.aip.org/content/aip/journal/apl/107/1?ver=pdfcov
Published by the AIP Publishing

APPLIED PHYSICS LETTERS **107**, 011902 (2015)

Controlling the plasmonic surface waves of metallic nanowires by transformation optics

Yichao Liu,[1] Jun Yuan,[1] Ge Yin,[1] Sailing He,[1,2] and Yungui Ma[1,a)]
[1]*State Key Laboratory of Modern Optical Instrumentation, Centre for Optical and Electromagnetic Research, College of Optical Science and Engineering, Zhejiang University, Hangzhou 310058, China*
[2]*Department of Electromagnetic Engineering, School of Electrical Engineering, Royal Institute of Technology, S-100 44 Stockholm, Sweden*

(Received 1 June 2015; accepted 23 June 2015; published online 6 July 2015)

In this letter, we introduce the technique of using transformation optics to manipulate the mode states of surface plasmonic waves of metallic nanowire waveguides. As examples we apply this technique to design two optical components: a three-dimensional (3D) electromagnetic mode rotator and a mode convertor. The rotator can rotate the polarization state of the surface wave around plasmonic nanowires by arbitrarily desired angles, and the convertor can transform the surface wave modes from one to another. Full-wave simulation is performed to verify the design and efficiency of our devices. Their potential application in photonic circuits is envisioned. © *2015 AIP Publishing LLC*. [http://dx.doi.org/10.1063/1.4926332]

Transformation optics is a powerful mathematical tool that can map empty geometries into concrete physical media parameterized by tensor properties under the form invariance of Maxwell equations. After the pioneering work on cloaks,[1–3] the inspired broad applications of this technique have greatly boosted the advancement of modern electromagnetics and produced numerous designs of electromagnetic (EM) devices with functionalities deemed impossible before, such as invisibility cloaks,[4–15] controlling plasmonics,[16–23] field concentrators,[24–27] field rotators,[27–30] transmutation of singularities,[31–34] and beam bends or expanders.[35]

Among these applications, controlling the wave state of polarization is very important in an optical circuit or system. In the literature,[28,29] Chen *et al.* first designed a two-dimensional (2D) transformation-medium shell that could rotate wave fields while remaining invisible. Sometime later, Kwon *et al.* improved this technique to design a 3D polarization rotator that could rotate the polarization state of an incoming beam in an empty space by arbitrary angles. These transformed devices were proposed for free-space applications.

In this letter, we make an attempt to apply this technique to manipulate the mode states of highly confined surface waves on metallic nanowires, which have attracted great research enthusiasms for their potential applications in nanophotonic circuits or devices.[36] As examples, we propose two component devices for nanowire waveguides: One is a rotator able to change the spatial polarizations of surface modes, and the other is a mode convertor that can transform the surface modes from one into another. In addition to scientific interests, the devices proposed here may find important practical applications in photonic circuits or optical interconnection systems.[37]

First, we discuss how to design a mode rotator for plasmonic nanowires placed in the air background. Without loss of the generality, we consider a silver nanowire of radius a and length l. Such a nanowire can guide different bounded surface modes along the cylindrical axis direction. As schematically shown in Fig. 1, an imagined donut-shaped EM rotator (yellow) with inner radius a, outer radius b, and length h ($h < l$) is positioned somewhere to surround the nanowire. When the surface waves enter this region, their spatial patterns will experience a gradual rotation around the z-axis and acquire a new and desired orientation state after passing the whole device.

Consider a cylindrical coordinate transformation from the electromagnetic into the physical spaces, i.e., $(\rho, \theta, z) \rightarrow (\rho', \theta', z')$.The above rotational function for the

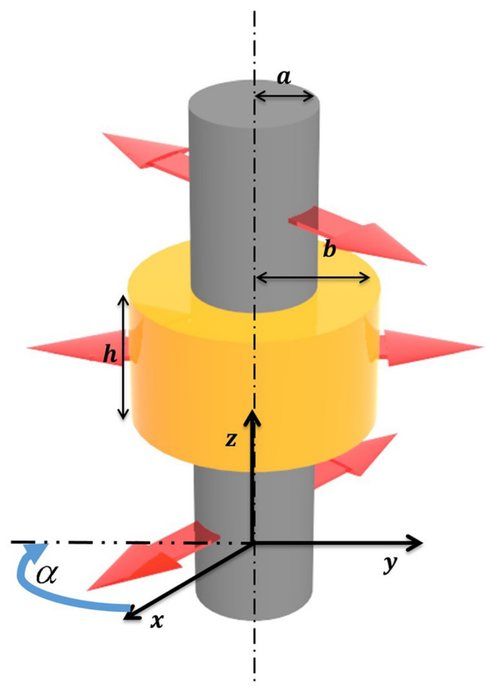

FIG. 1. Structural diagram of the surface wave rotator for nanowires. The gray rod is the silver nanowire, and the yellow cladding is the wave rotator. The red arrows represent the polarization directions at different positions along the propagation direction, which experiences a smooth change from x-axis to y-axis after passing the rotator.

a)Electronic mail: yungui@zju.edu.cn

imagined device can be realized by a simple mathematical mapping,

$$\rho' = \rho, \quad \theta' = \theta + \frac{\alpha(z - z_0)}{h}, \quad z' = z \quad \text{for } \rho \geq a \\ \text{and} \quad z_0 \leq z \leq z_0 + h, \tag{1}$$

where α is the rotation angle and z_0 is the coordinate of the lower edge of the device if we assume that the wave is incident from the bottom. No transformation is taken for the rest region. By this relationship, the permittivity and permeability tensors for this device are expressed by

$$\varepsilon = \mu = \begin{pmatrix} 1 & 0 & 0 \\ 0 & 1 + \rho^2\alpha^2/h^2 & \rho\alpha/h \\ 0 & \rho\alpha/h & 1 \end{pmatrix}. \tag{2}$$

In the following, we numerically examine the actual performance of this wave rotator by the simulation software of Comsol Multiphysics. The nanowire waveguide we consider here has a radius of 133 nm and a specific operation wavelength $\lambda = 400$ nm, which corresponds to a permittivity value $\varepsilon = -15.04 + 1.02i$ for silver.[38] The rotator has an outer radius of 266 nm, inner radius of 133 nm and length of 266 nm. With these parameters, different ordered surface modes could be excited traveling along the nanowire.[37] For the lowest three orders, their effective propagation constants are calculated to be 1.06, 0.99, and 0.79, respectively. For the simplicity of discussion, we consider the first mode with dipolar field distribution in the cross-section plane, which could be excited by properly defining the boundary condition for the input end. Here, we select $\alpha = \pi/2$, which means that the rotator will have a working angle of 90 degrees. This value can be modified by changing α. Fig. 2(a) provides a 3D view of the magnetic field in z direction along the nanowire axis. It is seen that the field pattern does show a gradual and finally 90° rotation after passing the rotator. The right side of Fig. 2(a) shows three cross-sectional magnetic field patterns at three z positions before the rotator, in the middle of the rotator, and after the rotator, respectively. Smooth rotation for the lowest eigenmode wave is clearly evidenced from these real-field distributions. We also examined and confirmed similar operation features for any higher order modes by this device, as shown in Fig. 2(b) for the second order mode. Note that our design is based on the assumption that the EM fields of the surface mostly exist inside the dielectric surrounding space, which is basically correct because the calculated skin depth for a silver film at $\lambda = 400$ nm is about 16 nm, far smaller than the decaying length of the surface mode in the dielectric surrounding. The full-wave simulation results show that this assumption works pretty well for surface wave modes.

The ideal transformed device works perfectly with an infinite thickness (i.e., $b \to \infty$). For evanescent surface waves with exponentially decreasing spatial amplitudes, it is practically possible to truncate the volume of the rotator for the purpose of easy application. An effective thickness dependent on the operation wavelength is expected. Fig. 3 plots the real rotation angle of the mode pattern after we physically truncate the rotator to have different thicknesses. It is seen that the truncated device can maintain the desired 90° rotation performance until its thickness $b - a = 0.25\lambda$. Below this limit, the real rotation angle decreases quickly. Three inset pictures on the top of Fig. 3 give the snapshots of the output magnetic field patterns corresponding to the rotators of thicknesses 0.1λ, 0.2λ, and 0.33λ, respectively. For the thickness smaller than the spatial decaying length of the eigenmode, the rotator can only partially cover the main electromagnetic fields and thus leads to a smaller rotation in the end. The effective thickness will be smaller for higher order modes that have larger spatial decaying constants.

Since we can manipulate the field polarization by rotating operation, a more interesting question comes to us that whether it is possible to transform eigenmodes among different orders, i.e., design a mode convertor. Generally, it will be very difficult because different eigenmodes are spatially orthogonal to each other. But, the strong spatial manipulation capability of transformation optics affords us a unique possible to do this. Here, as the proof of concept, we will try to design a convertor that can transform the first eigenmode of a nanowire into the second harmonic and vice versa. In the xy plance, the first and second eigenmodes of a nanowire have a dipolar and quadrupolar field distributions, as respectively shown by the cartoon pictures in Figs. 4(a) and 4(c),

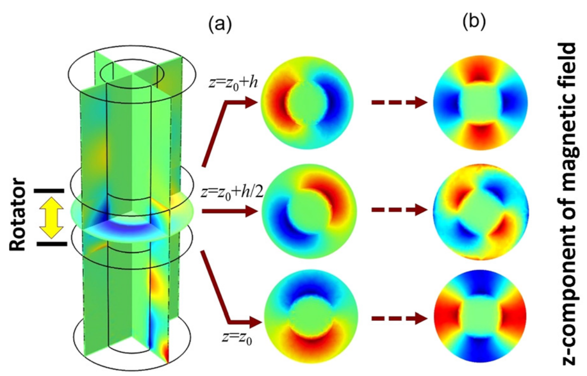

FIG. 2. Simulation of wave rotator operated on the first (a) and second order modes of a nanowire. In (a), the left is the 3D magnetic field pattern along the nanowire axis and the right insets give three cross-sectional field patterns in the xy plane at $z = z_0$, $z_0 + h/2$, and $z_0 + h$, respectively. In (b), the three patterns correspond to the real magnetic distributions at the same positions described in (a). The 90° rotation for the lowest eigenmode is evidenced.

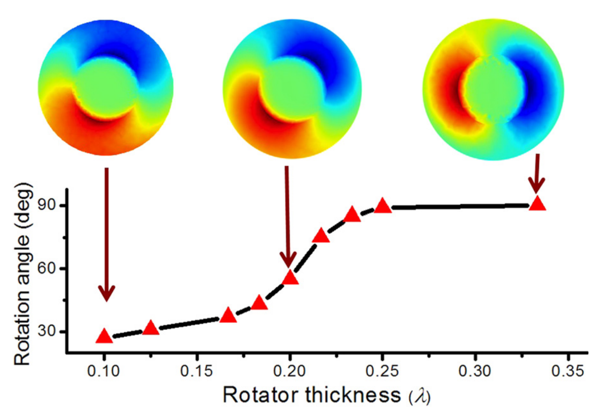

FIG. 3. Real rotation angle of the mode pattern for the truncated rotator as a function of the thickness. The top three figures are the normalized magnetic field in z direction for different rotator thickness. From left to right, the thickness is 0.1λ, 0.2λ, and 0.33λ, respectively.

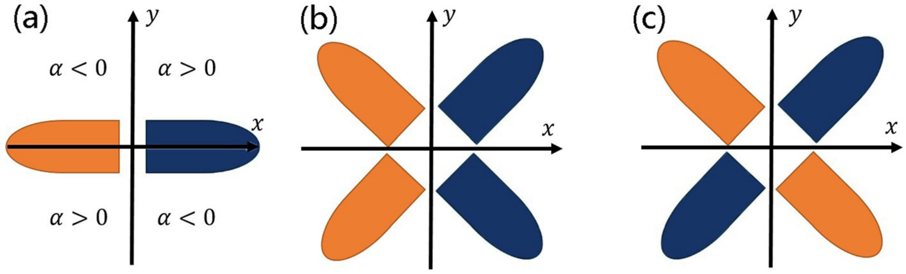

FIG. 4. Carton diagrams for the surface wave distributions around a silver nanowire in the xy plane. The orange and blue colors represent the positive and negative phases of a standing wave, respectively. (a) and (c) are for the patterns of the first and second eigenmodes, respectively. (b) is for an unstable middle state transformed by only applied Eqs. (1) and (3).

where the anti-phase features of the standing wave are distinguished by the colors (orange and blue). The most intuitive way to design such a convertor is to split and double the dipolar field distribution of the first eigenmode by applying a spatial stretching operation defined by

$$\alpha = \mathrm{sign}(xy)\alpha_0, \tag{3}$$

where $\alpha_0 = \pi/4$ and the rotation direction is dependent on the quadrature. By this operation, the convertor will give rise to a four-spot phase pattern as shown in Fig. 4(b) at the output end. But, this temporal field pattern is spatially not stable and will quickly merge together by transforming back into the incident dipolar mode.

Comparing the phase patterns in Figs. 4(b) and 4(c), we see that an additional phase difference by π between the regions of $y > 0$ and $y < 0$ is required to form a stable and quadrupolar field pattern. For this purpose, we assume the background materials of these two halves in the virtual space are different with refractive index $n = 1$ (i.e., air) for the region $y > 0$ and $n = n_0$ for the region $y < 0$. To yield a π phase difference, we should have

$$n_0 = 1 + \frac{\Lambda}{2h}, \tag{4}$$

where Λ is the wavelength of the surface wave. The transformation can be mathematically described by

$$\rho' = \frac{\rho}{n(y)}, \quad \theta' = \frac{1}{n(y)}\left[\theta + \frac{\alpha_0 \cdot \mathrm{sign}(xy)(z - z_0)}{h}\right],$$
$$z' = \frac{z}{n(y)} \quad \text{for } \rho \geq a \quad \text{and} \quad z_0 \leq z \leq z_0 + h, \tag{5}$$

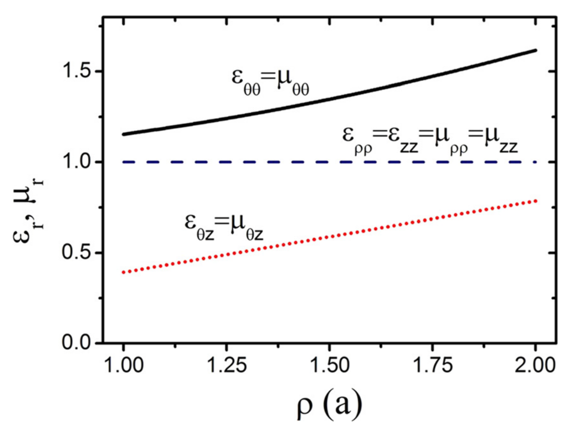

FIG. 5. Permittivity and permeability of the mode convertor in the half region $y > 0$. The black solid line represents the tensors $\varepsilon_{\theta\theta}, \mu_{\theta\theta}$, the dashed blue line represents the tensors $\varepsilon_{\rho\rho}, \varepsilon_{zz}, \mu_{\rho\rho}, \mu_{zz}$, and the red dotted line represents $\varepsilon_{\theta z}, \mu_{\theta z}$. The material parameters for the other half ($y < 0$) are exactly 1.76 times larger.

where $n(y) = 1$, for $y \geq 0$, and $n(y) = 1 + \frac{\Lambda}{2h}$, for $y < 0$. Applying Eq. (5), we could get the permittivity and permeability tensors of the convertor by Eq. (2) multiplied by an index factor n. In our example, the operating wavelength is 400 nm, $\Lambda = 404$ nm, and $n = 1.76$. Fig. 5 plots the radius dependence of the permittivity and permeability tensor elements of the convertor in the half with $y > 0$. Each tensor element for the other half is n times larger than these shown here. It is seen that all these parameters have reasonably moderate values without the singularity problems, thus providing a practical potential for the proposed device. The fabrication could be further facilitated if we imbedded the nanowire in a dielectric background.

The actual performance of the designed convertor is numerically inspected, as shown in Fig. 6(a), by the normalized 3D electric field pattern along the nanowire axis. The desired gradual evolution of the input mode is observed. For better visualization, three inset figures on the right side give the snapshots of the cross-sectional magnetic field distributions corresponding to the positions before, inside and after the convertor, respectively. These real-part field patterns clearly show the mode conversion feature of the designed device, i.e., transforming the first order mode into the second order of the nanowire. In our design, the virtual geometry of the convertor is assumed to be the combination of two identical halves but with different dielectric constants. This assumption will lead to additional boundary reflection for the surface waves touching the end surfaces of the convertor.

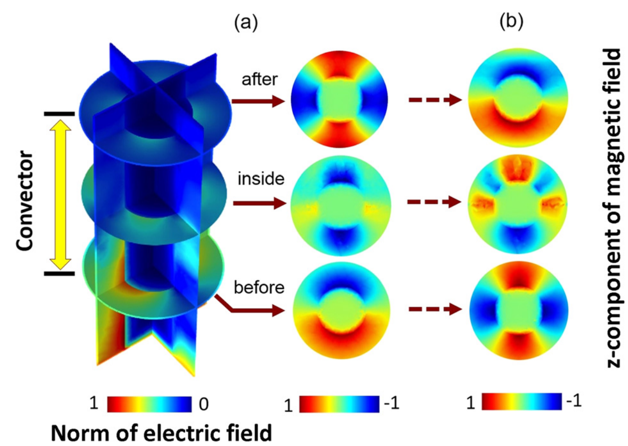

FIG. 6. Simulation of wave convertor inputted by the first (a) and second (b) order modes of a silver nanowire. In (a), the left gives a 3D view of the electric field magnitude along the nanowire, and the right gives the cross-sectional magnetic field patterns in the xy plane corresponding to the z positions before, inside and after the convertor, respectively. In (b), the three figures give the real magnetic field distributions at the position similarly defined in (a). The inter-mode conversion between the first two eigenmodes is evidenced.

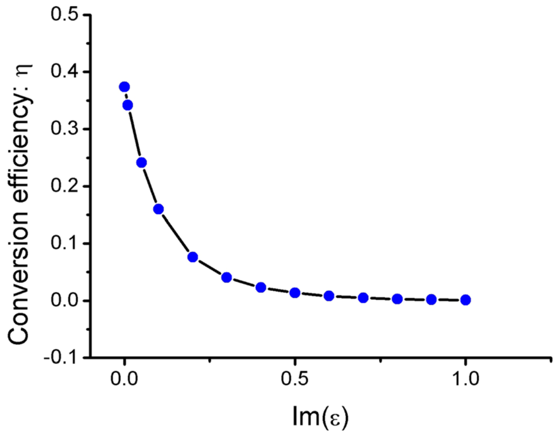

FIG. 7. Influence of the material loss to the conversion efficiency.

Here, we make a rough evaluation about the mode conversion efficiency by calculating the field intensity ratio η at the output end of the nanowire between the cases with and without the convertor. By integrating the field around a fixed circle, we get a value η around 0.374. This is a reasonable value, because the convertor we designed here is actually not a perfect one due to the existence of impedance mismatch and field distortion. The transformed fields after the convertor will form a stable mode only after passing a certain physical distance along the nanowire. In principle, this imperfection could be further controlled, for example, by properly choosing the refractive index n for the right half to minimize the interface mismatch. In addition, the same device can also transform the second order mode into the first order due to the transmission reciprocity, and it has the bidirectional conversion capability, as shown in Fig. 6(b). By properly refining the values of α and n in different spaces, it is both theoretically and technically fully possible to design a convertor that can transform the eigenmodes among arbitrary orders.

The mode rotator or convertor is designed to work for a specific frequency because their physical length is chosen according to the effective wavelength of the surface wave that depends on frequency. This point has been confirmed by our additional simulation (not shown here). Material loss for a real device is also a critical issue influencing the device efficiency. Fig. 7 plots the conversion efficiency of our mode convertor as a function of the imaginary part $\mathrm{Im}(\varepsilon)$ of permittivity. It is seen that η is sensitive to the loss and a good conversion performance can be achieved at $\mathrm{Im}(\varepsilon) < 0.1$.

In conclusion, we have demonstrated a mode rotator and a mode convertor that works for the optical plasmonic surface waves on metal nanowire. By simulation, we have analyzed the relations between the rotator thickness and its performance. We have also used the idea of rotator to design a mode convertor with acceptable conversion efficiency. The advantage of our two devices is their compact structures and convenient usage. One can integrate a nanowire waveguide with our devices and achieve some fascinating functions without resorting to some additional devices such as splitters and couplers. Of course, our devices have technical difficulties due to their complex material parameters. Nevertheless, with the rapid development of techniques, our devices will indeed have potential applications in optical interconnect systems for their space-saving characteristics.

The authors are grateful to the partial supports from NSFC (Grant Nos. 61271085, 60990322, 91130004, and 91233208), NSFC of Zhejiang Province (Grant No. LR15F050001), and Swedish VR Grant (Grant No. 621-2011-4620) and AOARD and the support by the Fundamental Research Funds for the Central Universities.

[1]J. B. Pendry, D. Schurig, and D. R. Smith, Science **312**, 1780 (2006).
[2]U. Leonhardt, Science **312**, 1777 (2006).
[3]J. B. Pendry, Prog. Electromagn. Res. **147**, 117 (2014).
[4]W. Cai, U. K. Chettiar, A. V. Kildishev, and V. M. Shalaev, Nat. Photonics **1**, 224 (2007).
[5] Alu and N. Engheta, Phys. Rev. Lett. **100**, 113901 (2008).
[6]J. Li and J. B. Pendry, Phys. Rev. Lett. **101**, 203901 (2008).
[7]R. Liu, C. Ji, J. J. Mock, J. Y. Chin, T. J. Cui, and D. R. Smith, Science **323**, 366 (2009).
[8]J. Valentine, J. Li, T. Zentgraf, G. Bartal, and X. Zhang, Nat. Mater. **8**, 568 (2009).
[9]B. Edwards, A. Alu, M. G. Silveirinha, and N. Engheta, Phys. Rev. Lett. **103**, 153901 (2009).
[10]T. Ergin, N. Stenger, P. Brenner, J. B. Pendry, and M. Wegener, Science **328**, 337 (2010).
[11]H. F. Ma and T. J. Cui, Nat. Commun. **1**, 21 (2010).
[12]X. Z. Chen, Y. Luo, J. J. Zhang, K. Jiang, J. B. Pendry, and S. Zhang, Nat. Commun. **2**, 176 (2011).
[13]Y. G. Ma, Y. C. Liu, L. Lan, T. T. Wu, W. Jiang, C. K. Ong, and S. L. He, Sci. Rep. **3**, 2182 (2013).
[14]L. H. Gabrielli, J. Cardenas, C. B. Poitras, and M. Lipson, Nat. Photonics. **3**, 461 (2009).
[15]B. L. Zhang, Y. Luo, X. G. Liu, and G. Barbastathis, Phys. Rev. Lett. **106**, 033901 (2011).
[16]P. A. Huidobro, M. L. Nesterov, L. Martín-Moreno, and F. J. García-Vidal, Nano Lett. **10**(6), 1985 (2010).
[17]Y. M. Liu, T. Zentgraf, G. Bartal, and X. Zhang, Nano Lett. **10**(6), 1991 (2010).
[18]Aubry, D. Y. Lei, A. I. AI Fernández-domínguez, Y. Sonnefraud, S. A. Maier, and J. B. Pendry, Nano Lett. **10**(7), 2574 (2010).
[19]Y. M. Liu and X. Zhang, Nanoscale **4**, 5277 (2012).
[20]M. Kadic, S. Guenneau, S. Enoch, P. A. Huidobro, L. Martín-Moreno, F. J. García-Vidal, J. Renger, and R. Quidant, Nanophotonics **1**, 51 (2012).
[21]J. Renger, M. Kadic, G. Dupont, S. S. Aćimović, S. Guenneau, R. Quidant, and S. Enoch, Opt. Express **18**, 15757 (2010).
[22]M. Kadic, S. Guenneau, and S. Enoch, Opt. Express **18**, 12027 (2010).
[23]M. Kadic, G. Dupont, S. Guenneau, and S. Enoch, J. Mod. Opt. **58**, 994 (2011).
[24]F. Sun and S. L. He, Prog. Electromagn. Res. **142**, 683 (2013).
[25]K. X. Liu, W. Jiang, F. Sun, and S. L. He, Prog. Electromagn. Res. **146**, 187 (2014).
[26]M. Rahm, D. Schurig, D. A. Roberts, S. A. Cummer, D. R. Smith, and J. B. Pendry, Photonics Nanostruct. Fundam. Appl. **6**, 87 (2008).
[27]Y. Luo, H. Chen, J. Zhang, L. Ran, and J. A. Kong, Phys. Rev. B **77**, 125127 (2008).
[28]H. Chen, B. Hou, S. Chen, X. Ao, W. Wen, and C. T. Chan, Phys. Rev. Lett. **102**(18), 183903 (2009).
[29]H. Y. Chen and C. T. Chan, Appl. Phys. Lett. **90**, 241105 (2007).
[30]D. H. Kwon and D. H. Werner, Opt. Express **16**(23), 18731 (2008).
[31]T. Tyc and U. Leonhardt, New J. Phys. **10**, 115038 (2008).
[32]Y. G. Ma, F. Sun, Y. Zhang, Y. Jin, and C. K. Ong, J. Opt. Soc. Am. A **29**, 124 (2012).
[33]J. Perczel, C. Garcia-Meca, and U. Leonhardt, J. Opt. **13**, 075103 (2011).
[34]Y. C. Liu, M. Mukhtar, Y. G. Ma, and C. K. Ong, J. Opt. Soc. Am. A **30**, 2280 (2013).
[35]M. Rahm, D. A. Roberts, J. B. Pendry, and D. R. Smith, Opt. Express **16**, 11555 (2008).
[36]X. Guo, Y. B. Ying, and L. M. Tong, Acc. Chem. Res. **47**, 656 (2014).
[37]X. Guo, Y. G. Ma, Y. P. Wang, and L. M. Tong, Laser Photonics Rev. **7**, 855 (2013).
[38]E. D. Palik, *Handbook of Optical Constants of Solids* (Academic Press, New York, 1991).